Self-contained on-chip fluid actuation for flow initiation in liquid cell transmission electron microscopy

Vivek Menon, Matthieu Denoual, Hiroshi Toshiyoshi, Hiroyuki Fujita

Japanese Journal of Applied Physics

The Japan Society of Applied Physics

RAPID COMMUNICATION • OPEN ACCESS

Self-contained on-chip fluid actuation for flow initiation in liquid cell transmission electron microscopy

To cite this article: Vivek Menon *et al* 2019 *Jpn. J. Appl. Phys.* **58** 090909

OPEN ACCESS

Japanese Journal of Applied Physics **58**, 090909 (2019) **RAPID COMMUNICATION**

https://doi.org/**10.7567/1347-4065/ab386a**

Self-contained on-chip fluid actuation for flow initiation in liquid cell transmission electron microscopy

Vivek Menon[1*], Matthieu Denoual[1,2,3], Hiroshi Toshiyoshi[1], and Hiroyuki Fujita[1]

[1]*Institute of Industrial Science, University of Tokyo, 4-6-1 Komaba Meguro-ku, Tokyo, Japan*
[2]*GREYC-ENSICAEN, Université de Caen Basse Normandie, 6 bd maréchal Juin, Caen 14000, France*
[3]*LIMMS, Institute of Industrial Science, 4-6-1 Komaba Meguro-ku, Tokyo, Japan*

[*]E-mail: vmenon@iis.u-tokyo.ac.jp

Received June 1, 2019; revised July 30, 2019; accepted August 5, 2019; published online August 21, 2019

Liquid cells for transmission electron microscopy enable the observation of liquid samples with nanometer resolution, but sample activity must often be triggered via external stimuli including liquid flow and mixing. Existing devices enable flow using specialized TEM holders and external pumping setups which limits technique accessibility. Here, a liquid cell with integrated MEMS valves and pumps is demonstrated with flow capabilities using an electrical-contact holder. On-chip electrochemical pumps and capillary burst valves allow for the injection of fluid from an integrated reservoir into an observation chamber using only electrical signals from a general microchip-sized TEM holder.

Supplementary material for this article is available online

Transmission electron microscopy (TEM) is a powerful and ubiquitous observational technique that can allow for the high-resolution imaging of materials and samples in real-time. Nanometer-scale resolutions are regularly achievable with conventional TEM techniques, while sub-nanometer resolutions have been demonstrated both theoretically and practically in specialized situations.[1–3] These properties make TEM an attractive option to investigate the nanoscale dynamics behind biological and chemical processes and reactions. However, these systems usually require a wet or gaseous environment as well as some degree of external stimulus in order to exhibit such activity. While the environment of the TEM column makes it well-suited to the study of isolated non-volatile specimens in high-vacuum, specialized techniques are necessary to view samples in the presence of liquids and initiate observable reactions. In this paper, a new pressure-based mechanism is proposed to induce in situ liquid flow during TEM observation without the use of a specialized TEM holder.

Environmental TEM techniques have been applied to observe samples in gaseous environments using differential pumping to investigate solid–gas interface dynamics.[4,5] Another technique uses fully encapsulated millimeter-scale gas chambers located at the tip of the TEM specimen holder to view samples in the presence of atmospheric-pressure gases.[6–9] The same method has been applied to contain liquid-phase samples within the TEM holder as well. Such devices utilize sandwiched chips with electron-transparent membranes placed in the TEM specimen holder that contain the volatile sample while still allowing the imaging beam to pass through the liquid sample.[10–13] This fundamental technique, known as liquid cell TEM (LCTEM) enables the imaging of samples in a liquid environment which can allow for the observation of the dynamics of time-dependent reactions and systems, but requires more advanced functionality in order to interact with the sample during observation.

Due to the small volumes contained within liquid cell chambers, usually on the order of nanoliters or picoliters, it is beneficial to be able to trigger target reactions during TEM observation on demand as spontaneous reactions will often run to completion before the sample can be observed. Electrochemical reactions have been frequently studied using LCTEM with devices incorporating electrodes used in conjunction with TEM holders featuring electrical interconnects.[14,15] Various temperature-dependent reactions have also been studied using heating elements integrated into TEM holders as well as on the liquid cell directly.[16,17] In order to initiate or sustain spontaneous reactions, it is necessary to control the concentration of reactions within the sample chamber. Functionally, this is achieved through the generation of fluid flow within the liquid cell structure. Liquid cell devices designed for use with highly-specialized TEM holders featuring fluidic conduits within the holder body can be used to flow fluid across the sample with external pumps.[18–20] Initial devices required designing and building a custom setup, however currently several commercial TEM specimen holders are available that are capable of applying flow through the holder body from external pumps as well as mixing input reactants before they enter the observable region of the TEM.[21–23]

While the holder-based flow LCTEM devices described above are capable of supplying flow to the sample, the layout of the sealing system allows a significant amount of the liquid to flow around the observable region rather than through it.[24] This in conjunction with the length of tubing running out of the TEM chamber and through the external pumping systems can delay desired changes in the reactant composition and hinder accurate estimations of concentrations. Furthermore, existing LCTEM flow devices require either the custom fabrication of a specialized flow-capable TEM holder or the purchase of such equipment. This represents a significant barrier to entry for researchers interested in studying liquid-phase nanoscale reactions but without access to such highly-specific TEM equipment. By utilizing micro electromechanical systems (MEMS) technology, some of the flow capabilities exhibited by existing holder-flow systems can be integrated directly onto the liquid cell device and activated using a simpler TEM holder with only electrical interconnects.

In the device described here, fluid from a built-in reservoir within the cell itself can be pumped into the observable region of the cell using an on-chip electrochemical pump and burst valve structure. Rather than the continuous-flow paradigm of existing LCTEM flow devices, here we propose a device structure in which reactants are kept in separate chambers with closed microfluidic valves while TEM observation is established and subsequently flowed together in situ using integrated pumps. The valve structures used here are based on capillary burst valves that utilize a hydrophobic region within a hydrophilic chamber to inhibit fluid flow until a sufficient forward pressure is applied.[25,26] In order to initiate flow past the burst valves, the forward pressure is generated using electrochemical pumps based on microfluidic devices that use electrolysis to produce gas and thereby create a pressure gradient within a channel.[27–29] By combining these components in a liquid cell that fits within the area available on a TEM holder using MEMS integration techniques, the ability to initiate flow within TEM can be achieved without the use of a specialized flow-capable holder.

The basic liquid cell structure, based on the geometry established by other previously reported LCTEM devices, consists of two micromachined silicon chips bonded together, each featuring thin silicon-nitride membranes that allow for transmission of the TEM electron beam when a fluid sample is encapsulated in the gap between them. The sample is confined between the two chips by a patterned spacer layer that defines a narrow channel with reservoirs at each end. The novel activity of the device is achieved through the integration of valve and pump structures. A patterned hydrophobic barrier that crosses the channel near its center serves as a valve that separates the channel into two chambers. This layer prevents flow along the channel between the two chambers until initiated by the user. Each chamber is accessible via an inlet hole in the reservoir area and is flanked by a pair of electrodes that serve as pumps to induce flow in either direction within the channel. A schematic view of the liquid cell as well as the TEM holder in which it fits can be seen in Fig. 1.

The chips are fabricated by first depositing a 50–70 nm thick film of stoichiometric Si_3N_4 via LPCVD on 200 μm thick Si wafers. The intrinsic stress within the stoichiometric Si_3N_4 limits out-of-plane bowing or buckling of the membranes during fabrication, assembly, and use. The electrodes are formed with a 100 nm thick platinum layer that is deposited via sputtering and patterned with a lift-off process. The channel separator feature is then created using lift-off to pattern a 300 nm thick hydrophobic fluorocarbon layer formed from C_4F_8 plasma. A second 700 nm thick fluorocarbon layer is deposited and patterned to form the spacer that defines the channel. The backside silicon is then etched using a combination of deep reactive ion etching and isotropic SF_6 plasma etching to reveal the silicon-nitride membrane in the center of the chips and etch out the loading inlets. Plasma-based release limits degradation of the front-side features and was found to be more controllable and process-compatible as compared to KOH etching which was also explored. The membranes used here are approximately 80 μm wide to match the largest viewing window of the TEM system (HD-2300, Hitachi) as well as curved to reduce potential stress concentrations. Figure 2 shows a single

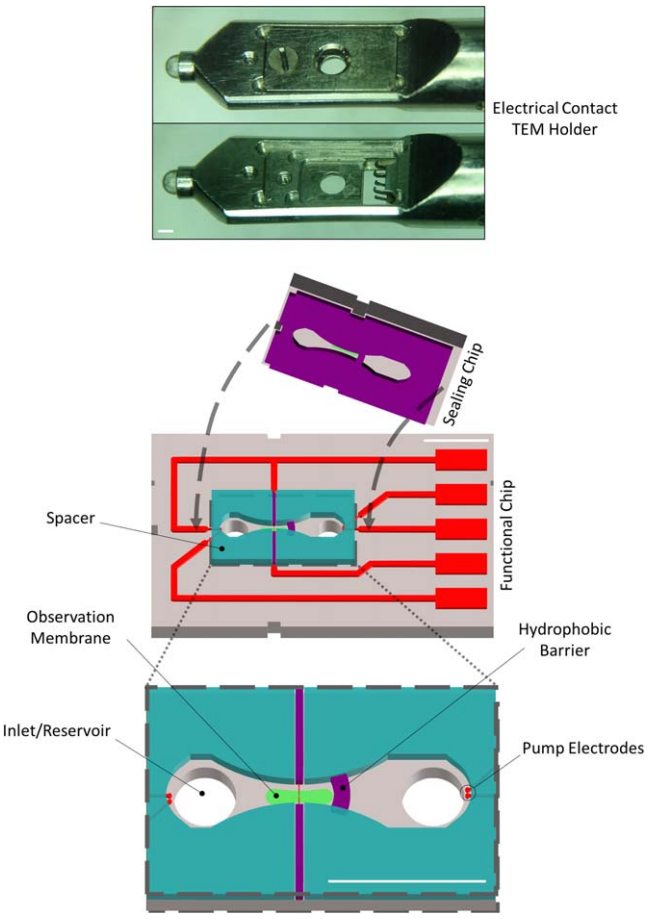

Fig. 1. (Color online) (top) Tip of TEM specimen holder with cover attached (above) and cover removed (below) showing the electrical-interconnect pins. (bottom) Schematic illustration of the unassembled liquid cell device. The inlay shows a zoomed view where the electron-transparent TEM membrane and fluidic channel can be seen. Scales = 1 mm.

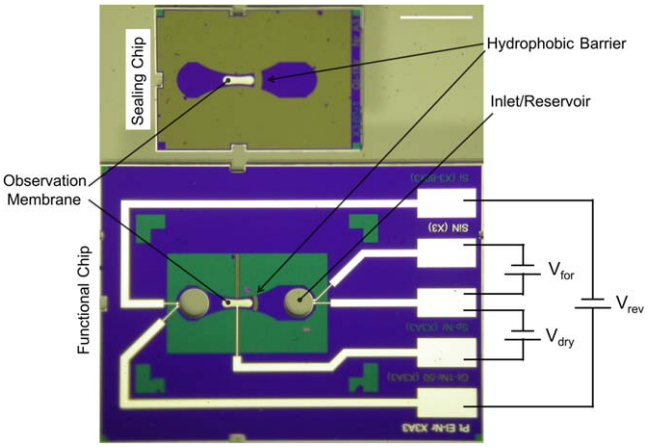

Fig. 2. (Color online) Device chips with off-membrane hydrophobic barriers as fabricated. The electrical contacts on the right side of the functional chip can be used to drive flow within the central channel through the application of voltage through the TEM holder interconnects. V_{for} will drive fluid from the right chamber to the left, while V_{rev} will do the opposite. V_{dry} will cause the generation of gas directly on the observation membrane which can be used to dry the area after it has been filled with liquid. Scale = 1 mm.

functional chip as fabricated before bonding. Devices were fabricated with hydrophobic barriers located upstream of the observation membrane as shown in Figs. 1 and 2 as well as directly on the membrane itself. This second type of device

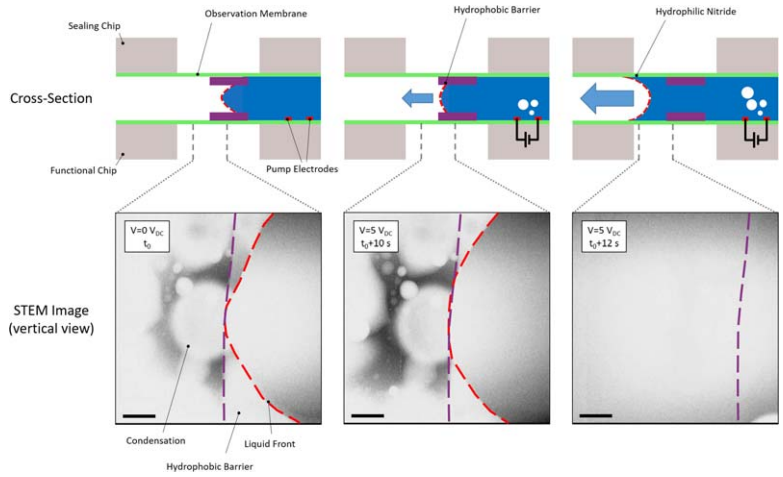

Fig. 3. (Color online) Progression of sample pinning and filling in liquid cell with hydrophobic barriers located directly on the observation membrane. (top) Schematic cross-sectional view of the observable region of the device in the initial state (left), during pumping (center), and after release of the burst valve (right). Liquid samples are loaded in the right chamber and are prevented from flowing into the left chamber by the hydrophobic barrier. When sufficient voltage is applied across the pump electrodes, gas is generated within the chamber and the fluid is forced across the barrier until it reaches the hydrophilic nitride on the other side and is drawn into the left chamber through capillary action. (bottom) Dark field Z-contrast STEM view of the hydrophobic barrier during pump actuation. The liquid on the right is initially pinned in place until voltage is applied to the pump electrodes. The liquid front bulges toward the left until it finally fills the chamber in the last pane. Scales = 10 μm. A real-time video available in supplementary video 1 is available online at stacks.iop.org/JJAP/58/090909/mmedia.

enables the direct observation of liquid gating events as shown in Fig. 3. A corresponding sealing chip is also fabricated on the same wafer, and can be manually aligned under an optical microscope and bonded to the functional chip using UV-cured epoxy. If necessary, samples may be deposited and dried on the nitride membrane before bonding the two chips together using a micropipette to position the sample droplet. Particles or materials deposited directly on the viewing in this way membrane will usually remain immobile due to surface adhesive forces even when a sample liquid is flowed over it during operation of the liquid cell. This can be useful for studying the evolution of a particular analyte particle in the presence of a sample solution over time, for example. The individual chips as fabricated can be seen in Fig. 2.

Once assembled, liquid samples can be loaded using a micropipette into either of the device chambers via the two loading inlets. The channel formed by the bonded chips and the spacer layer is approximately 1 μm tall and varies from 250–500 μm in width with an overall length of 2 mm. Aside from the spacer sidewalls, the surface of the liquid chamber is made of stoichiometric Si_3N_4, as mentioned above. The relatively hydrophilic nitride, with an average measured surface contact angle of 44° with water, allows water-based sample liquids placed at the device inlets to enter and readily fill the chamber through capillary action.

The capillary pressure ΔP of the liquid during filling can be approximated with the Young–Laplace equation as follows in Eq. (1).

$$\Delta P = \gamma\left(\frac{1}{R_w} + \frac{1}{R_h}\right) \tag{1}$$

Here γ is the surface tension of the sample while R_w and R_h are the radii of curvature for the solid–liquid interface for the channel width and height, respectively. Expressed in terms of the measured contact angle θ and the channel width w and height h, these radii are as follows:

$$R_w = \frac{w}{2\cos\theta_w},\ R_h = \frac{h}{2\cos\theta_h} \tag{2}$$

The capillary forces within the channel structure can be approximated using the above formulae following the guide of previous works investigating liquids in microchannels.[30,31] For water within the channel, capillary attraction generates a forward pressure of approximately 1×10^5 Pa at the liquid front which draws the sample into the chamber. When the advancing liquid reaches the hydrophobic barrier in the center of the channel, flow is impeded. With an average measured surface contact angle of 113° and a pattern width of 250 μm, the liquid is pinned in place by a back pressure of approximately 6×10^4 Pa. This immobilizes the liquid front, thereby ensuring that samples loaded into one chamber will not spread to the other prematurely. The immobilizing back pressure is derived from the surface properties of the channel, and as such future devices can be fabricated with thinner channels which would serve to increase the maximum achievable TEM resolution without significantly interfering with the device's pinning capability. Once the device chamber has been thus filled with a sample fluid, it can then be sealed by applying epoxy to the inlets. The filled and sealed device is then ready to be loaded into the TEM holder and viewed in TEM.

Once loaded into TEM, water-based samples and/or electrolytes confined to one chamber by the hydrophobic barrier can be flowed into the other using the pump electrodes near the chamber reservoirs. The application of sufficient voltage between the platinum pump electrodes flanking a chamber loaded with an aqueous solution can initiate electrolysis.[32]

$$2H_2O \rightarrow 4H^+ + 4e^- + O_2$$

$$2H_2O + 2e^- \rightarrow 2OH^- + H_2$$

With a sustained voltage, the production of oxygen and hydrogen continues with the products dissolving within the

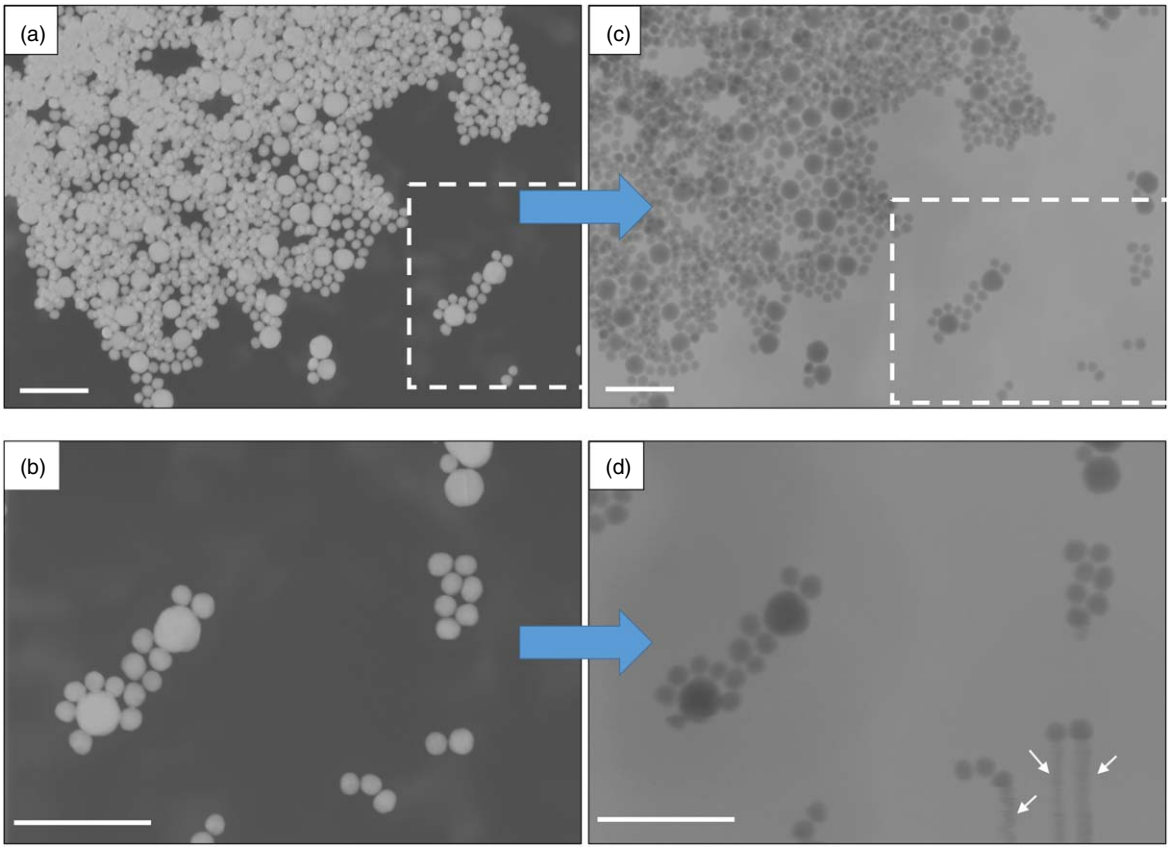

Fig. 4. (Color online) In situ wetting of gold nanoparticles in dark field Z-contrast STEM to demonstrate in situ sample immersion capability. (a) Dried 50 and 100 nm diameter gold nanoparticles in the liquid cell. (b) Magnified view of white outlined area in (a). (c) View of the same region of the liquid cell in (a) after solution was flowed into it using the onboard pumping feature. The lighter background now represents the solution as viewed with dark field Z-contrast imaging. (d) Magnified view of white outlined area in (d). Arrows indicate streaks where particles have undergone movement due to the longer electron beam dwell time at higher magnification and slower imaging speed. Scales = 300 nm.

sample solution. Once the solution is saturated in the vicinity of the electrodes, oxygen and hydrogen will evolve from the liquid solution as a gas in the form of bubbles. Continued electrolysis causes existing bubbles to grow and the nucleation of new ones as more oxygen and hydrogen is produced. The gasses evolved from the solution serve to displace the liquid and thereby increase the pressure within the confined volume of the chamber. When the generated pressure exceeds the back pressure of the hydrophobic gate, the solution begins to propagate over the pattern. Once the liquid front reaches the end of the pattern, it comes into contact with the hydrophilic nitride of the channel once again and capillary forces draw the solution through to enter and fill the downstream chamber. This process is outlined schematically and can be seen directly in Fig. 3. In this way, when a chamber of the device has been loaded with a sample, it is maintained in that chamber until the forward pump is activated and the sample is driven to fill the second chamber.

As described above, this device is capable of initiating liquid flow from one chamber to the other during TEM observation. This ability can be used to observe the first moments of a reaction of an analyte when exposed to a sample solution. The analyte can first be immobilized on the observation membrane surface before the device is assembled. The cell can then be filled and sealed with the sample solution contained in the second chamber. The whole device can then be loaded into TEM and the initial state of the analyte can be observed. When desired, the sample solution can be flowed into the chamber with the immobilized analyte, and any resulting activity can be directly observed from the instant the reaction begins. In order to demonstrate this kind of experimental protocol as well as the resolution of the device in both the wet and dry state a test solution of 50 and 100 nm diameter gold nanoparticles was used. The colloid was first dried on the observation membrane to immobilize the nanoparticles on the surface as observation targets. The device was then assembled and the same solution was loaded into the inlet and reservoir separate from the observation membrane. After sealing, the device was loaded into an electrical-interconnect TEM holder and inserted into the STEM vacuum chamber for observation using the dark field Z-contrast imaging mode. The immobilized gold nanoparticles were first observed as loaded in the dry state. Without interrupting the TEM observation, a ramping voltage of 3–5 V was applied across the electrodes flanking the solution-filled chamber over the course of 30 s until activity was observed and the voltage was stopped. Upon the introduction of liquid, an overall contrast inversion was observed due to the increased Z-contrast signal of the liquid, but as can be seen in Fig. 4, the same region of immobilized nanoparticles could be observed in both the initial dry and subsequent wet states with minimal loss of resolution. This type of experiment can potentially be used to observe the incubation of an analyte in a reactive solution, enabling the capture of both the initial moments of the reaction as well as subsequent activity all without the use of a specialized flow-capable TEM holder.

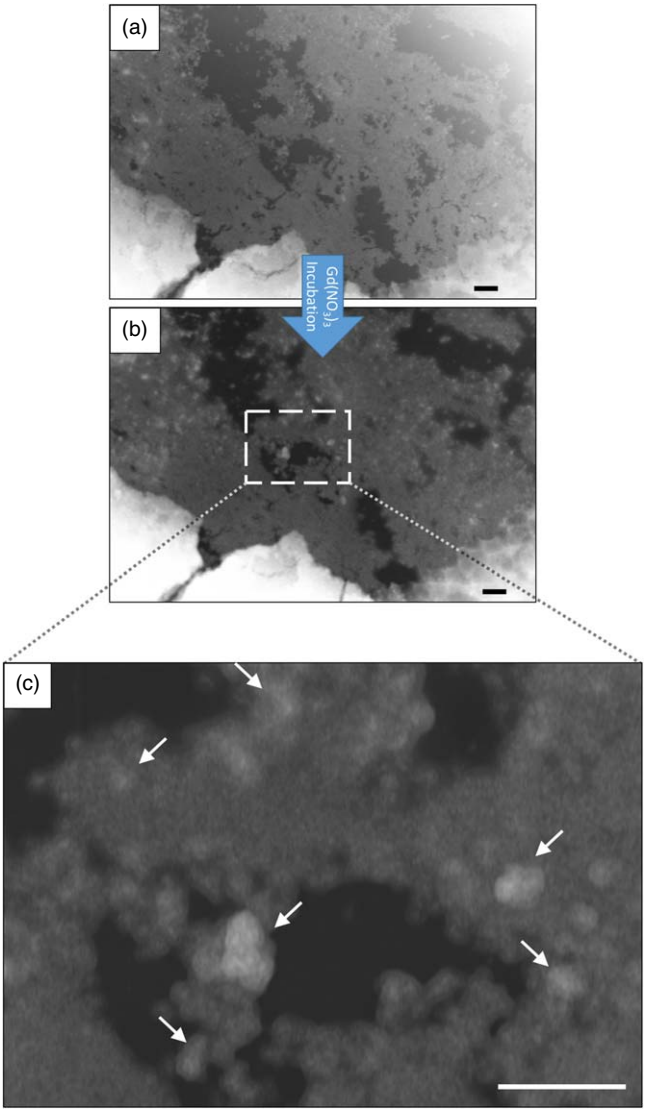

Fig. 5. (Color online) Demonstration of wetting and drying capabilities of the device through the observation of zeolite structures before and after incubation in gadolinium nitrate. The liquid cell can be used to introduce a sample solution to an observed region as well as subsequently dry that same region within a continuous TEM observation session. (a) Initial dark field Z-contrast STEM view of dry zeolites on the liquid cell membrane. The disperse zeolite nanostructures are the grey cloudy features. (b) Same region as (a) after 2 h of incubation in gadolinium nitrate and in situ drying. (c) Magnified view of region in (b) with arrows showing locations of increased signal developed after incubation. Scales = 1 μm.

Another demonstration experiment was performed using a sample of faujasite zeolite. Zeolite nanoparticles are of scientific interest for use in applications ranging from catalysis to medical imaging.[33,34] In this experiment, the ability for sodium-ion-laden faujasite nanostructures to undergo ion exchange in the presence of gadolinium ions was to be explored. A solution of faujasite nanoparticles with Na^+ ions was dried on the membrane of a liquid cell device to immobilize the zeolite structures for observation. The device was assembled and the opposing chamber was filled with a solution of $Gd(NO_3)_3$. After sealing and loading into the STEM, the dry zeolite structures were initially observed. The gadolinium nitrate solution was then flowed over the immobilized zeolites which were allowed to incubate in the presence of Gd^{3+} ions for approximately 2 h. While observation was continued during this period, the zeolite structures were not large or dense enough to be resolved in the wet state. In order to view the results of the experiment, an additional electrode located on the observation membrane of the liquid cell device was used to trigger electrolysis of the solution at the center of the device. Voltage was applied continually until a gas bubble formed within the observation region of the device large enough to displace the liquid and dry the zeolites for viewing. This procedure was performed without removing the sample from TEM and continual observation was performed. After incubation and in situ drying, the zeolites exhibited concentrated regions of higher contrast than the initial state as can be seen in Fig. 5, which could potentially be a result of increased signal due to replacement of Na^+ ions with heavier Gd^{3+} ions. While further experimentation would be necessary to confirm these results, this experiment demonstrates the advanced flow manipulation capabilities of the liquid cell device.

The liquid cell device introduced here features a mechanism to induce flow that has not yet been incorporated into LCTEM devices. The utilization of electrochemical pumps eliminates the need for external pumping apparatus and flow-capable holders while hydrophobic burst valves enable the induction of flow from an initially dry state. By avoiding the use of specialized holders, the device proposed here is compatible with a wider range of TEM setups for researchers without access to LCTEM-focused. Furthermore, while flow-capable holders would have difficulty applying fluid to an initially dry sample without the formation of unwanted bubbles due to the high fluidic resistance of the liquid cell geometry, the device described here allows for the direct injection of a controlled volume into the experimental chamber reliably and without visible bubbling. While continuous-flow experiments remain limited to dedicated flow LCTEM holders, the liquid cell described here provides unique functionality in a more accessible package.

Acknowledgments The authors would like to thank Nicolas Lobato-Dauzier for assistance in preliminary proof-of-concept experimentation as well as Dr. Julien Grand and Dr. Svetlana Mintova for supplying zeolite samples and expertize. LPCVD was performed with support at the Micro System Integration Center (μSIC, Tohoku University) while mask fabrication and wafer dicing was performed at the VLSI Design and Education Center (VDEC, University of Tokyo). The authors acknowledge funding of Grant-in-Aid for Fundamental Research A (Grant No. JP17H01049) from the Japan Society for the Promotion of Science.

ORCID iDs Vivek Menon https://orcid.org/0000-0002-9038-9536

1) P. Baston, N. Dellby, and O. Krivanek, Nature **418**, 617 (2002).
2) J. Barthel and A. Thust, Phys. Rev. Lett. **101**, 200801 (2008).
3) R. Erni, M. D. Rossel, C. Kisielowski, and U. Dahmen, Phys. Rev. Lett. **102**, 1 (2009).
4) E. Boyes and P. Gai, Ultramicroscopy **67**, 219 (1997).
5) R. Sharma and K. Weiss, Microsc. Res. Tech. **42**, 270 (1998).
6) G. Parkinson, Catal. Lett. **2**, 303 (1989).
7) S. Giorgio, S. Sao Joao, S. Nitsche, D. Chaudanson, G. Sitja, and C. Henry, Ultramicroscopy **106**, 503 (2006).
8) J. Creemer, S. Helveg, G. Hoveling, S. Ullmann, A. Molenbroek, P. Sarro, and H. Zandbergen, Ultramicroscopy **108**, 993 (2008).
9) N. de Jonge, W. C. Bigelow, and G. M. Veith, Nano Lett. **10**, 1028 (2010).
10) M. J. Williamson, R. M. Tromp, P. M. Vereecken, R. Hull, and F. M. Ross, Nat. Mater. **2**, 532 (2003).
11) K.-L. Liu, C.-C. Wu, Y.-J. Huang, H. Peng, H.-Y. Chang, P. Chang, L. Hsu, and T.-R. Yew, Lab Chip **8**, 1915 (2008).
12) H. Zheng, S. A. Claridge, A. M. Minor, A. P. Alivisatos, and U. Dahmen, Nano Lett. **9**, 2460 (2009).

13) J. M. Grogan and H. H. Bau, J. Microelectromech. Syst. **19**, 885 (2010).
14) A. Radisic, P. M. Vereecken, J. B. Hannon, P. C. Searson, and F. M. Ross, Nano Lett. **6**, 238 (2006).
15) M. Egawa, T. Ishida, L. Jalabert, and H. Fujita, Appl. Phys. Lett. **108**, 023104 (2016).
16) H. L. Xin and H. Zheng, Nano Lett. **12**, 1470 (2012).
17) E. R. White, M. Mecklenburg, S. B. Singer, S. Aloni, and B. C. Regan, Appl. Phys. Express **4**, 055201 (2011).
18) N. de Jonge, D. B. Peckys, G. J. Kremers, and D. W. Piston, Proc. Natl Acad. Sci. USA **106**, 2159 (2009).
19) E. A. Ring and N. de Jonge, Microsc. Microanal. **16**, 622 (2010).
20) C. Mueller, M. Harb, J. R. Dwyer, and R. J. D. Miler, J. Phys. Chem. Lett. **4**, 2339 (2013).
21) "Protochips Poseidon Select", Protochips [https://protochips.com/products/poseidon-select/]. (accessed: November 30, 2018).
22) "Hummingbird Scientific Liquid Flow," Hummingbird Scientific [http://hummingbirdscientific.com/products/liquid/]. (accessed: November 30, 2018).
23) "DENSsolutions Stream", DENSsolutions [https://denssolutions.com/products/stream/]. (accessed: November 30, 2018).
24) F. M. Ross, *Liquid Cell Electron Microscopy* (Cambridge University Press, New York, 2017), p. 49.
25) B. Zhao, J. S. Moore, and D. J. Beebe, Anal. Chem. **74**, 4259 (2002).
26) Y. Feng, Z. Zhou, X. Ye, and J. Xiong, Sens. Actuators A **108**, 138 (2003).
27) D. O'Keefe, C. O'Herlihy, Y. Gross, and J. G. Kelly, Br. J. Anaesth. **73**, 843 (1994).
28) S. Böhm, W. Olthuis, and P. Bergveld, Biomed. Microdevices **1**, 121 (1999).
29) J. W. Munyan, H. V. Fuentes, M. Draper, R. T. Kelly, and A. T. Woolley, Lab Chip **3**, 217 (2003).
30) N. Ichikawa, K. Hosokawa, and R. Maeda, J. Colloid Interface Sci. **280**, 155 (2004).
31) V. N. Phan, N.-T. Nguyen, C. Yang, P. Joseph, L. Djeghalf, D. Bourrier, and A.-M. Gue, Langmuir **26**, 13251 (2010).
32) P. W. Atkins, J. De Paula, and J. Keeler, *Atkin's Physical Chemistry* (Oxford University Press, Oxford, 2018) 11th ed.
33) S. Mintova, J. Grand, and V. Valtchev, C. R. Chim. **19**, 183 (2016).
34) H. Awala, J.-P. Gilson, R. Retoux, P. Boullay, J.-M. Goupil, V. Valtchev, and S. Mintova, Nat. Mater. **14**, 447 (2015).